JOURNAL OF GUIDANCE, CONTROL, AND DYNAMICS
Vol. 33, No. 4, July–August 2010

Hybrid Steering Logic for Single-Gimbal Control Moment Gyroscopes

Frederick A. Leve* and Norman G. Fitz-Coy*,†
University of Florida, Gainesville, Florida 32611

DOI: 10.2514/1.46853

The development of a hybrid steering logic that maintains attitude tracking precision while avoiding hyperbolic internal singularities or escaping elliptic singularities inherent to single-gimbal control moment gyroscopes is discussed. The hybrid steering logic enables null motion and limits torque error when approaching a hyperbolic internal singularity, or it adds torque error and limits null motion when approaching an elliptic internal or external singularity. The hybrid-steering-logic algorithm accomplishes these tasks through the definitions of novel singularity metrics that transition continuously from local-gradient to pseudoinverse methods when moving from hyperbolic to elliptic singularities. Analysis and simulations are presented to demonstrate the performance of the hybrid steering logic as compared with the two legacy methods. The development and results are applied to a four-single-gimbal-control-moment-gyroscope pyramid arrangement with a skew angle of $\theta = 54.74$ deg.

Nomenclature

$\mathbf{A}$	=	Jacobian
$\mathbf{A}^+$	=	Moore–Penrose pseudoinverse
c, k	=	controller gains
$\mathbf{d}$	=	control-moment-gyroscope null-motion vector
$\mathbf{e}$	=	spacecraft quaternion error vector elements
e_{ss}	=	steady-state attitude error in degrees
$\mathbf{e}_4$	=	spacecraft quaternion error scalar element
$\mathbf{h}$	=	control-moment gyroscope angular momentum vector
$\dot{\mathbf{h}}$	=	control-moment gyroscope output torque vector
h_0	=	magnitude of nominal angular momentum
$\mathbf{J}$	=	spacecraft centroidal inertia tensor
m	=	singularity measure
$\mathbf{N}$	=	null-space basis for the Jacobian
$\mathbf{P}$	=	projection matrix for singularity metric
$\mathbf{Q}$	=	singularity definition matrix
$\mathbf{U}$	=	left unitary matrix found from singular value decomposition of jacobian
$\mathbf{V}$	=	left unitary matrix found from singular value decomposition of Jacobian
α_0, β_0	=	hybrid-steering-logic singularity parameter amplitudes
γ	=	singularity parameter
δ	=	column matrix of gimbal angles
$\dot{\delta}$	=	column matrix of gimbal rates
θ	=	skew angle of control-moment-gyroscope pyramid
μ, γ_0	=	singularity parameter decay rate and amplitude
μ_1, a	=	hybrid-steering-logic singularity parameter decay rate and amplitude for α
μ_2, b	=	hybrid-steering-logic singularity parameter decay rate and amplitude for β
σ_i	=	ith singular value of Jacobian
τ	=	control-moment-gyroscope internal control torque vector
ω	=	spacecraft angular velocity vector
$\tilde{\omega}$	=	skew symmetric matrix of the spacecraft angular velocity vector

Received 24 August 2009; revision received 7 March 2010; accepted for publication 23 March 2010.

*Graduate Student, Department of Mechanical and Aerospace Engineering.

†Associate Professor, Department of Mechanical and Aerospace Engineering.

I. Introduction

CONTROL moment gyroscopes (CMGs) are used in spacecraft attitude control when propellant is not abundant and rapid retargeting and precision pointing are desired (e.g., earth monitoring, blue force tracking, laser communication, and space science missions). CMGs and reaction wheels (RWs) are capable of the highest pointing precision, although CMGs are known to provide higher slew rates and torque output for the same amount of power.

CMGs can be classified as those with multiple and single controllable degrees of freedom (DOF). One such class of multiple DOF actuators, known as double-gimbal CMGs (DGCMGs), are the most massive and mechanically complex class of CMGs. They use an additional gimbal, which contributes an extra controllable DOF for producing torque. However, these actuators suffer from gimbal lock, where the gimbal axes align and the extra degree of freedom is lost [1]. Singularity avoidance strategies for DGCMGs have been studied and proven effective [2–4].

Variable-speed CMGs (VSCMGs) have an extra controllable DOF through modes where the CMG's flywheels are accelerated (i.e., RW mode). The RW modes of these actuators provide the needed torque when at singularity. In addition, VSCMGs provide the advantage of storing the kinetic energy of the flywheels as they are spun down to operating speed when transitioning from RW to CMG modes. Studies of these devices for power storage purposes has been reported in literature [5–9]. A drawback, however, is the loss of torque amplification as a consequence of the added DOF. In addition, the variable speeds of their flywheels make it difficult to isolate unwanted vibration, such as jitter, and in some cases may even be the cause of it [10]. An effective method exists that uses null motion to reduce the amount of RW mode used and, therefore, addresses some of the concerns about these actuators [11–13].

The least mechanically complex CMGs are the single-gimbal CMGs (SGCMGs). These actuators contain a single controllable DOF through rotation of a constant-speed flywheel about a gimbal axis. Inherent to all CMGs is the property of torque amplification (i.e, they produce more net torque output for a given gimbal motor torque), with SGCMGs having the highest amount. However, SGCMGs suffer from internal singularities (see Sec. II). At these singularities, the torque vectors of the SGCMGs lie in a plane, whereby torque is unavailable out of this plane. These singularities are difficult to deal with due to the sole controllable DOF for SGCMGs. To avoid or escape these configurations, a steering logic must be used.

The amount of torque amplification present in SGCMGs is what is considered most favorable in this research; therefore, a steering law for SGCMGs is developed that reduces torque error while maintaining torque amplification. This steering law is know as the

hybrid steering logic (HSL), which combines the local-gradient (LG) and pseudoinverse methods to provide a hybrid sense of singularity avoidance and escape. What is meant by hybrid is that there is a transition from null motion of a LG method to torque error from a pseudoinverse when moving from a hyperbolic to elliptic singularity.

II. Singularities

A. External Singularities

External or saturation singularities are phenomena associated with the maximum projection of the CMG angular momentum. When these singularities occur, the resulting angular momentum from the CMG system is at its maximum magnitude for its direction and, as a consequence, additional CMG angular momentum in this direction is not possible. A surface, analogous to that of a work space for robotics, is defined for the maximum amount of CMG angular momentum of the system. This surface, shown in Fig. 1, is known as the external singular surface or momentum envelope. It is found by the summation of the CMG angular momenta at the singular states [14,15]. External singularities occur at points on or outside this surface.

B. Internal Singularities

The output torque of the CMG system can be found by differentiating the resultant CMG angular momentum vector with respect to time, resulting in

$$\dot{\mathbf{h}} = \frac{\partial \mathbf{h}}{\partial \delta}\dot{\delta} = h_0 \mathbf{A}(\delta)\,\dot{\delta} \tag{1}$$

where h_0 is the magnitude of individual CMG angular momentum and $\mathbf{A}(\delta)$ is the Jacobian. The Jacobian is a nonlinear function of the gimbal angles δ and is the kinematic mapping that relates the gimbal states to the CMG output torque. Internal singularities are kinematic phenomena that occur at specific sets of gimbal angles when the Jacobian is singular (i.e., $\mathbf{A}$ is not full column rank). At an internal singularity, the torque vectors for each CMG are coplanar, eliminating the possibility of producing torque normal to the plane. These singularities are instantaneous and can degrade attitude tracking precision.

There are essentially two types of internal singularities, hyperbolic and elliptic, which are categorized by the possibility of null motion near them. Null motion is defined as motion applied from the CMG

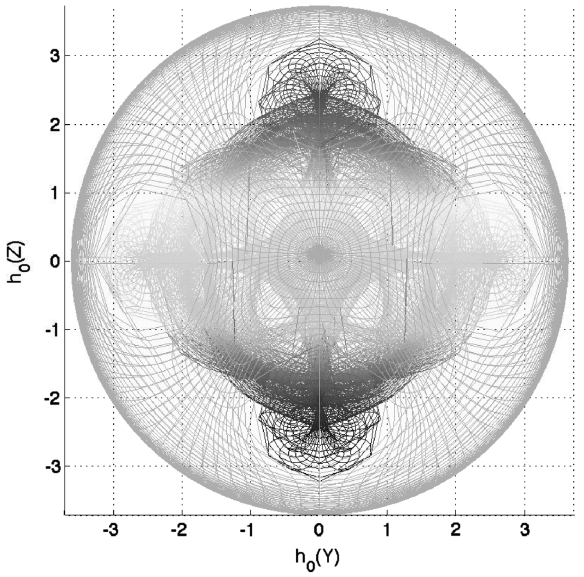

a) Momentum envelope (top view)

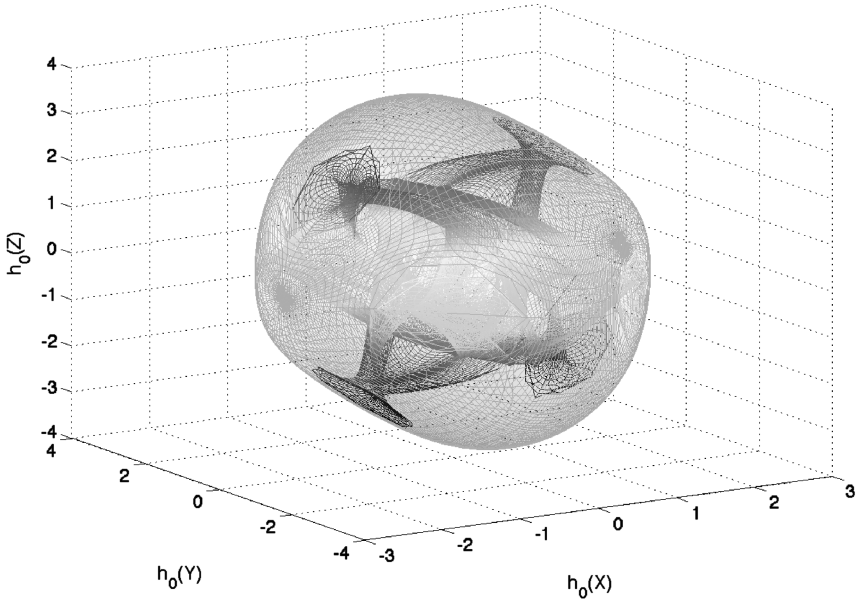

b) Momentum envelope (isometric view)

Fig. 1 Four-CMG angular momentum envelope, including internal singular surfaces for a pyramid arrangement at $\theta = 54.74$ deg.

gimbals that produces no torque on the spacecraft. In essence, every point on the angular momentum space that is not a singularity for the Jacobian, or is at least at a hyperbolic singularity, has infinite solution of gimbal angles due to null space. On the other hand, elliptic internal and external singularities only have one solution to the corresponding point on the angular momentum space and, therefore, cannot be escaped by null motion. There are degenerate cases of hyperbolic internal singularities where there is null set of gimbal angles for a specific point on the momentum space, although every solution in the set is singular (i.e., corresponds to a singular Jacobian); therefore, no escape through null motion is possible. It is assumed in this paper that the four-CMG pyramid arrangement is free of degenerate hyperbolic internal singularities. Topology and differential geometry are typically used to represent hyperbolic and elliptic internal singularities as surfaces or manifolds [10,16]. The behavior of singularities can also be explained through the use of linear algebra. For the linear algebra approach, a Taylor series expansion of the CMG angular momentum about a singular configuration gives

$$\mathbf{h}(\delta) - \mathbf{h}(\delta^S) = \sum_{i=1}^{n}\left[\left.\frac{\partial \mathbf{h}_i}{\partial \delta_i}\right|_{\delta_i^S}\Delta\delta_i + \frac{1}{2}\left.\frac{\partial^2 \mathbf{h}_i}{\partial \delta_i^2}\right|_{\delta_i^S}\Delta\delta_i^2 + \text{HOT}\right] \tag{2}$$

where HOT are higher-order terms of the series, and $\mathbf{h}(\delta^S)$ is the angular momentum at a singular set of gimbal angles δ^S and $\Delta\delta_i = \delta_i - \delta_i^S$.

The first term on the right-hand side (RHS) of Eq. (2) contains the ith column of the Jacobian $\hat{\mathbf{a}}_i = (\partial \mathbf{h}_i/\partial \delta_i)|_{\delta_i^S}$, which is associated with the ith CMG's torque direction. The second term on the RHS contains the partial derivative of the Jacobian's ith column with respect to the ith gimbal angle $(\partial^2 \mathbf{h}_i/\partial \delta_i^2)|_{\delta_i^S}$. From Eq. (1),

$$\dot{\hat{\mathbf{a}}}_i = \frac{\partial \hat{\mathbf{a}}_i}{\partial \delta_i}\dot{\delta}_i = \dot{\delta}_i\,\hat{\delta}_i \times \hat{\mathbf{a}}_i = -\dot{\delta}_i h_i \hat{\mathbf{h}}_i \tag{3}$$

$$\frac{\partial^2 \mathbf{h}_i}{\partial \delta_i^2} = \frac{\partial \hat{\mathbf{a}}_i}{\partial \delta_i} = -h_i \hat{\mathbf{h}}_i = -\mathbf{h}_i \tag{4}$$

where $\hat{}$ denotes a unit vector. Next, we project Eq. (2) onto the singular direction $\mathbf{s} = \text{null}(\mathbf{A}^T)$ and manipulate, using Eqs. (3) and (4), to yield

$$\mathbf{s} \cdot [\mathbf{h}(\delta) - \mathbf{h}(\delta_S)] \backsimeq -\frac{1}{2}\sum_{i=1}^{n} \mathbf{h}_i \cdot \mathbf{s}\Delta\delta_i^2 \tag{5}$$

where the first term on the RHS of Eq. (2) is zero because of the definition of the singular direction (i.e, $\mathbf{As} = \mathbf{0}$). Equation (5) can be written more compactly as

$$\mathbf{s} \cdot [\mathbf{h}(\delta) - \mathbf{h}(\delta_S)] = -\tfrac{1}{2}\Delta\delta^T \mathbf{P}\Delta\delta \tag{6}$$

where the projection matrix $\mathbf{P} = \text{diag}(\mathbf{h}_i \cdot \mathbf{s})$.

By definition, null motion does not affect the total angular momentum; then, with $\mathbf{h}(\delta) - \mathbf{h}(\delta_S)$, the difference is always zero. Using this property, the left-hand side (LHS) of Eq. (6) at null motion is zero (i.e., $\mathbf{h}(\delta) = \mathbf{h}(\delta^S) \Rightarrow \Delta\delta_i^T \mathbf{P}\Delta\delta_i = 0$). The null motion is expressed in terms of the basis $\mathbf{N} = \text{null}(\mathbf{A})$ as follows:

$$\Delta\delta = \sum_{i=1}^{[n-r(\mathbf{A})]} \lambda_i \nu_i = \mathbf{N}\lambda \tag{7}$$

where λ is a column matrix of the scaling components of the null-space basis vectors ν_i, and $\mathbf{N} \in \mathbb{R}^{n\times[n-r(\mathbf{A})]}$ is the dimension of the null-space basis for any system of CMGs with $r(\mathbf{A}) = \text{rank}(\mathbf{A})$. Substituting Eq. (7) into Eq. (6) yields

$$\mathbf{0} = \lambda^T \mathbf{N}^T \mathbf{P}\mathbf{N}\lambda = \lambda^T \mathbf{Q}\lambda \tag{8}$$

Since the definition of elliptic and hyperbolic singularities depend on the existence of null vectors, $\mathbf{Q}$ can be used to classify the singularities. If $\mathbf{Q}$ is definite (i.e., has all positive or negative eigenvalues), there is no existence of a null vector λ that satisfies Eq. (8) [17].

When $\mathbf{Q}$ is semidefinite (i.e., it has at least one zero eigenvalue), then a null space exists with $\lambda \neq \mathbf{0}$ that satisfies Eq. (8). Therefore, null motion is possible near singularity, and singularities may be avoidable [18]. If the matrix $\mathbf{Q}$ is indefinite (i.e., the eigenvalues are positive and negative), the result of Eq. (8) has the possibility of being equal to zero, as seen in the example below:

$$\lambda^T \mathbf{Q}\lambda = [\lambda_1 \quad \lambda_2]\begin{bmatrix}1 & 0\\ 0 & -1\end{bmatrix}\begin{bmatrix}\lambda_1\\ \lambda_2\end{bmatrix} = \lambda_1^2 - \lambda_2^2 = 0 \tag{9}$$

where $\lambda_1 = \lambda_2$. In this case, null motion is also possible near singularity. Recall that there are degenerate hyperbolic internal singularities, which cannot be escaped by null motion.

To summarize, hyperbolic singularities are those where null motion exists (i.e., any point on the momentum space has infinite solutions of gimbal angles, some of which are not a sufficient condition for a mathematically singularity of the Jacobian). Singularities of this type correspond to $\mathbf{Q}$ being semidefinite or indefinite. Elliptic singularities are those that do not have null solutions (i.e., only a single set of gimbal angles for that point on the momentum space that corresponds to a mathematical singularity of the Jacobian). Singularities of this type correspond to $\mathbf{Q}$ being definite.

III. Steering Laws

Steering laws can be broken down to three main groups: singularity avoidance, singularity escape, and hybrid algorithms known as singularity avoidance and escape. These groups, as well as the subgroups associated with them, are shown in Fig. 2. The HSL is a singularity avoidance and escape algorithm that is formulated from already well-known singularity avoidance algorithms known as LG methods and a singularity escape algorithm known as singular direction avoidance (SDA).

A. Singularity Avoidance Algorithms

Singularity avoidance methods either use null motion or constrain the gimbal angles to avoid internal singularities locally and real time or globally from an offline calculation of singularity-free null-motion trajectories [19–24]. Because these methods use either null motion or traverse a singularity-free region of the momentum envelope, they do not induce torque error and are typically the most precise. Honeywell has patented methods that do not explicitly use null space but that implicitly do so by creating constraints that keep the gimbals away from singularity without needing to recognize their presence explicitly [25–27]. A simple example is the steering logic for scissored pairs, where mere constraints are used to keep the array out of trouble. These are able to guarantee singularity avoidance and an available torque but reduce the available work space of the system by requiring it to be singularity free [28,29].

B. Singularity Escape Algorithms

Singularity escape methods, known as pseudoinverse solutions, add torque error to pass through or escape an internal singularity [30–33]. These methods do not take into consideration the type of internal singularity that is being approached. Dismissing this knowledge eliminates the possibility of avoiding or escaping hyperbolic internal singularities through null motion, which reduces the amount of torque error. Torque error is not desired for precision attitude control; thus, there is merit in minimizing it.

C. Singularity Escape and Avoidance Algorithms

Singularity escape and avoidance algorithms use the traits of singularity avoidance and singularity escape algorithms. These algorithms either try to use null motion or a constrained set of gimbal angles to avoid singularities whenever possible, but they induce torque error when the tradeoff of performance is in favor of induced torque error versus the constraining of the CMG momentum (e.g.,

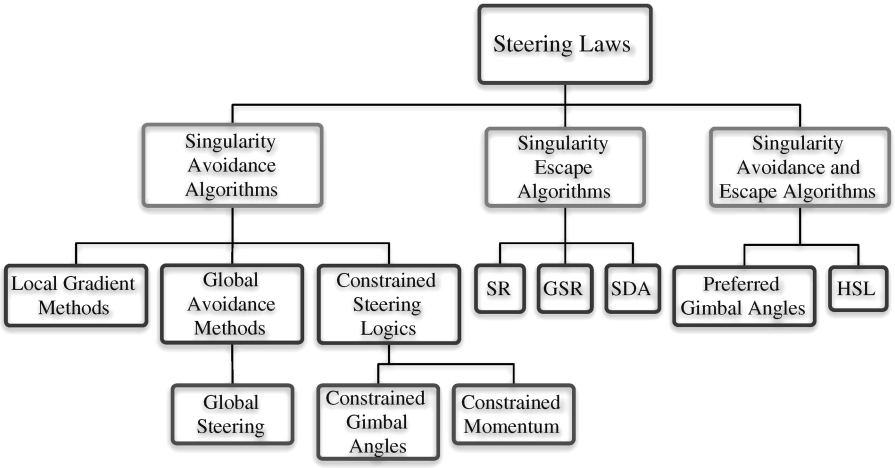

Fig. 2 Steering law breakdown.

example could be when the mission requirements are for high torque and slew rates, but there is a more relaxed constraint on the torque error allowed in pointing). An example of such a steering algorithm uses preferred gimbal angles. Preferred gimbal angles are a set of initial gimbal angles for SGCMGs that can be reached by null motion. These angles are preferred, since maneuvers originating from them avoid a singular configuration [34].

IV. Hybrid Steering Logic

Existing steering logics do not explicitly consider the type of internal singularity that is being encountered; thus, they do not completely address attitude tracking performance of SGCMG attitude control systems. The proposed HSL uses the knowledge of the type of singularity encountered (i.e., elliptic and hyperbolic internal singularities) to improve the attitude tracking performance of the SGCMG attitude control system. By using a hybrid approach, HSL acts as a LG method (i.e., null motion for singularity avoidance) at hyperbolic internal singularity and the SDA method (i.e., pseudoinverse solutions for singularity escape) at elliptic singularity. The challenge is to develop the appropriate singularity metrics, such that the LG and SDA components of the hybrid strategy do not counteract each other during operation.

A. Internal Singularity Metrics

Further development considers a four-CMG pyramid arrangement with a skew angle of $\theta = 54.74$ deg. The singularity metrics α and β used in HSL are defined as

$$\alpha = \alpha_0 e^{-a\bar{\alpha}} e^{-\mu_1 m} \tag{10}$$

$$\beta = \beta_0 e^{-b\bar{\beta}} e^{-\mu_2 m} \tag{11}$$

where a, b, μ_1, μ_2, α_0, and β_0 are positive scalar constants, and

$$m = \sqrt{\det(\mathbf{A}\mathbf{A}^T)} \tag{12}$$

At singularity, this system has $\mathbf{Q} \in \mathbb{R}^{2\times 2}$; therefore, the $\det(\mathbf{Q})$ will be zero or negative (i.e., $\mathbf{Q}$ is semidefinite or indefinite) for hyperbolic internal singularities and positive (i.e., $\mathbf{Q}$ is definite) for elliptic singularities. Taking this into account, parameters $\bar{\alpha}$ and $\bar{\beta}$ are defined as

$$\bar{\alpha} = |Q_0 - \det(\mathbf{Q})| \tag{13}$$

$$\bar{\beta} = \frac{1}{|Q_0 - \det(\mathbf{Q})|} = \frac{1}{\bar{\alpha}} \tag{14}$$

where Q_0 is a scalar value chosen on the same order of magnitude of $\det(\mathbf{Q})$ but greater to scale the response of $\bar{\alpha}$ and $\bar{\beta}$. It is important to note that the constant parameters a, b, μ_1, μ_2, α_0, and β_0 are used to morph the HSL steering logic into the LG and SDA methods. For example, if the parameters $a = b = \alpha_0 = 0$ and $\beta_0 \neq 0$, then the HSL method is the LG method. Therefore, choosing metrics α and β in this way ensures that null motion will be added when approaching an internal singularity that is hyperbolic, and torque error with less null motion will be added when approaching an internal singularity that is elliptic.

B. Steering Logic

The proposed steering logic is defined as

$$\dot{\delta} = \frac{1}{h_0}\mathbf{A}^{\mathrm{SDA},\alpha}\dot{\mathbf{h}} + \beta[\mathbf{1} - \mathbf{A}^{+}\mathbf{A}]\mathbf{d} \tag{15}$$

where $\mathbf{A}^{\mathrm{SDA},\alpha}$ is

$$\mathbf{A}^{\mathrm{SDA},\alpha} = \mathbf{V}\begin{bmatrix} \frac{1}{\sigma_1} & 0 & 0 \\ 0 & \frac{1}{\sigma_2} & 0 \\ 0 & 0 & \frac{\sigma_3}{\sigma_3^2+\alpha} \\ 0 & 0 & 0 \end{bmatrix}\mathbf{U}^T \tag{16}$$

The difference between the conventional $\mathbf{A}^{\mathrm{SDA}}$ and $\mathbf{A}^{\mathrm{SDA},\alpha}$ is the parameter that regulates σ_3. In $\mathbf{A}^{\mathrm{SDA}}$, the regulation parameter is γ, which is

$$\gamma = \gamma_0 e^{-\mu m} \tag{17}$$

with positive constants γ_0 and μ, but with $\mathbf{A}^{\mathrm{SDA},\alpha}$, the singularity parameter is α [defined in Eq. (10)], which regulates the amount of induced torque error in the vicinity of elliptic singularities. Through a singular value decomposition (SVD) of $\mathbf{A}$, Eq. (15) can be written as

$$\dot{\delta} = \frac{1}{h_0}\mathbf{A}^{\mathrm{SDA},\alpha}\dot{\mathbf{h}} + \beta\left[\mathbf{1} - \mathbf{V}\begin{bmatrix} \mathbf{1} & \mathbf{0} \\ \mathbf{0}^T & 0 \end{bmatrix}\mathbf{V}^T\right]\mathbf{d} \tag{18}$$

Here, the null-motion projection matrix is expressed as a function of nonsingular matrices, because the matrix $\mathbf{V}$ is unitary and, thus, always invertible. Also, very robust numerical algorithms exist for computing the SVD, so its computational risk in a real-time implementation is not particularly high.

The scalar that regulates the magnitude of the null motion is β. The null vector $\mathbf{d}$ is in the direction of the gradient of $f = -\det(\mathbf{A}\mathbf{A}^T) = -m^2$ and maximizes the distance from singularity.

This choice of this function reduces the computation needed for the gradient {i.e., the derivative of $[-\det(\mathbf{A}\mathbf{A}^T)]$ is simpler than the derivative $\sqrt{(\det(\mathbf{A}\mathbf{A}^T)}$} and ensures that the addition of null motion will not approach infinity at the region of singularity (i.e., $\frac{1}{m} \to \infty$ as $m \to 0$). It should be mentioned that the null vector is a nonlinear

Table 1 Simulation model parameters

Variable	Value	Units
$\mathbf{J}$	$\begin{pmatrix} 100 & -2 & 1.5 \\ -2 & 900 & 60 \\ 1.5 & -60 & 1000 \end{pmatrix}$	kgm^2
θ	54.74	deg
$\mathbf{e}_0$	$[0.043555 \quad 0.087105 \quad 0.043555 \quad 0.99430]^T$	——
ω_0	$[0 \quad 0 \quad 0]^T$	deg /s
h_0	128	Nms
k	0.05	Nm
c	0.15	Nms
e_{ss}	0.001	deg
Δt	0.02	s

function of the gimbal angles and is simplified due to the symmetry of the four-CMG pyramid arrangement.

V. Simulation Results

To evaluate the performance of the proposed HSL against heritage steering logics (i.e., LG and SDA), simulations were performed using a four-SGCMG system in a pyramidal configuration. To ensure a fair comparison, the control logic and satellite model were identical for all simulations. For each steering logic, three different scenarios were simulated: 1) starting in a zero-momentum $\delta = [0 \quad 0 \quad 0 \quad 0]^T$ deg (i.e., far from singularity), 2) starting near an elliptic external singularity $\delta = [105 \quad 105 \quad 105 \quad 105]^T$ deg, and 3) starting near a hyperbolic internal singularity $\delta = [15 \quad 105 \quad 195 \quad -75]^T$ deg. The singularity conditions were verified for each case by the singularity measure defined in Eq. (12). Performance measures compared are 1) the transient response of the error quaternion, 2) the amount and duration of singularity encounter, 3) the magnitude of gimbal rate, 4) the amount of torque error (i.e., $\dot{\mathbf{h}} - h_0\mathbf{A}\dot{\delta}$) for singularity escape, and 5) null-motion contribution. Additionally, α, β, and det($\mathbf{Q}$) are also considered.

The Jacobian associated with this pyramidal configuration is

$$\mathbf{A} = \begin{bmatrix} -c(\theta)c(\delta_1) & s(\delta_2) & c(\theta)c(\delta_3) & -s(\delta_4) \\ -s(\delta_1) & -c(\theta)c(\delta_2) & s(\delta_3) & c(\theta)c(\delta_4) \\ s(\theta)c(\delta_1) & s(\theta)c(\delta_2) & s(\theta)c(\delta_3) & s(\theta)c(\delta_4) \end{bmatrix} \tag{19}$$

where $\theta = 54.74$ deg was used for a near-spherical momentum envelope. The associated angular momentum vector is

$$\mathbf{h} = h_0 \begin{bmatrix} -c(\theta)s(\delta_1) - c(\delta_2) + c(\theta)s(\delta_3) + c(\delta_4) \\ c(\delta_1) - c(\theta)s(\delta_2) - c(\delta_3) + c(\theta)s(\delta_4) \\ s(\theta)(s(\delta_1) + s(\delta_2) + s(\delta_3) + s(\delta_4)) \end{bmatrix} \tag{20}$$

All simulations are performed using a fourth-order fixed-time-step Runga–Kutta, with the parameters shown in Table 1. The actuator parameters chosen for this simulation are associated with the Honeywell M95 SGCMGs, which are sized for the satellite system chosen for simulation [35].

A. Simulation Parameters

It should be noted that care must be taken when numerically defining the singular direction, because $\mathbf{s} = \mathbf{0}$ when the system has a full rank Jacobian. Because the rank is also found numerically, a tolerance should be set on the singularity measure to determine what is considered full rank. For the results presented in this paper, rank deficiency for the HSL was defined as $m \leq 0.5$. The simulations terminate when the steady-state error e_{ss} is achieved:

$$e_{ss} = \min[2\sin^{-1}(\|\mathbf{e}\|), 2\pi - 2\sin^{-1}(\|\mathbf{e}\|)] \tag{21}$$

This equation is used to find the value of the error angle associated with the error in the attitude between two frames. A value of e_{ss} is chosen, because it is known that CMGs can have a pointing precision on the order of one-thousandth of a degree [36].

B. Case 1: At Zero-Momentum Configuration

The first set of simulations has initial gimbal angles at $\delta = [0 \quad 0 \quad 0 \quad 0]^T$ deg, far away from internal singularities.

Typically, CMG systems are spun up from a zero-momentum configuration, as shown in Fig. 3, for a pyramidal four-CMG cluster. For this arrangement, the net angular momentum of the CMGs is zero and the system is far from internal singularity.

1. *Local Gradient Simulation Results*

The parameters for this simulation are $\alpha_0 = a = b = \mu_1 = 0$ and $\mu_2 = \beta_0 = 1$. The results in Figs. 4a and 4d show that the LG method was able to perform the maneuver to the given error tolerance e_{ss} without encountering singularity. The null motion shown in Fig. 4f is small but significant when compared with the total output gimbal rates in Fig. 4b. This is due to the small value for the internal singularity metric of β, shown in Fig. 4h. The value of det($\mathbf{Q}$), shown in Fig. 4i, is zero, since the singular direction is undefined and the Jacobian has full rank and confirms the results shown in Fig. 4d.

2. *Singular-Direction-Avoidance Simulation Results*

The parameters for this simulation are $\alpha_0 = 0.01$, $\beta_0 = a = b = \mu_2 = 0$, and $\mu_1 = 1$. The SDA method shows similar results in the transient response of the states to that of the LG method at the cost of torque error, shown in Fig. 5c. This is due to the small value of the internal singularity metric α, shown in Fig. 5g. There is no singularity encounter for this simulation, which is verified in the Figs. 5d and 5i, where the det($\mathbf{Q}$) = 0.

3. *Hybrid-Steering-Logic Simulation Results*

The parameters for this simulation are $\alpha_0 = 0.01$, $\beta_0 = 2$, $a = 1$, $b = 3$, and $\mu_1 = \mu_2 = 1$. The HSL method contains similar results to that of the SDA and LG methods, although the torque error in Fig. 6c added into the system is still smaller than that of SDA, and the null motion in Fig. 6f is smaller than that of the LG method. This method has nonzero values for both of the new internal singularity metrics α and β in Figs. 6g and 6h, respectively, because both null motion and torque error are added. This simulation is verified to have not encountered singularity through the value of m in Fig. 6d and a zero value of det($\mathbf{Q}$) in Fig. 6i.

C. Case 2: Near-Elliptic External Singularity

The second set of simulations starts at initial gimbal angles $\delta = [105 \quad 105 \quad 105 \quad 105]^T$ deg, which are near an elliptic saturation singularity at (i.e., 15 deg for each CMG away from the internal singularity $\delta = [90 \quad 90 \quad 90 \quad 90]^T$ deg).

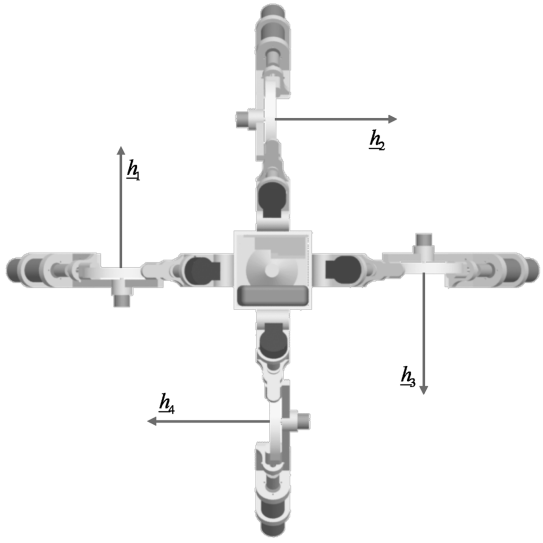

Fig. 3 Zero-momentum configuration of a four-CMG cluster in a pyramid arrangement.

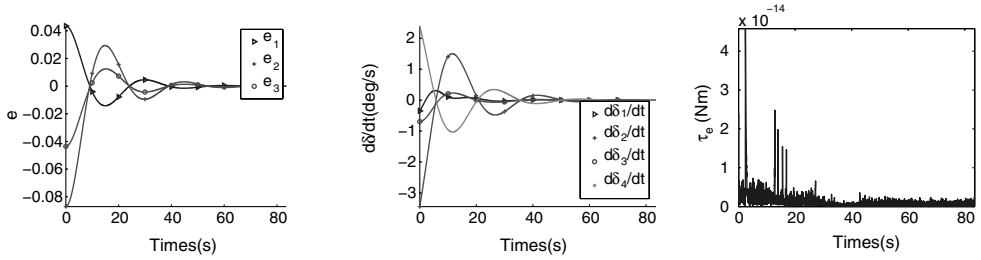

a) Quaternion error vector elements b) CMG gimbal rates c) Torque error

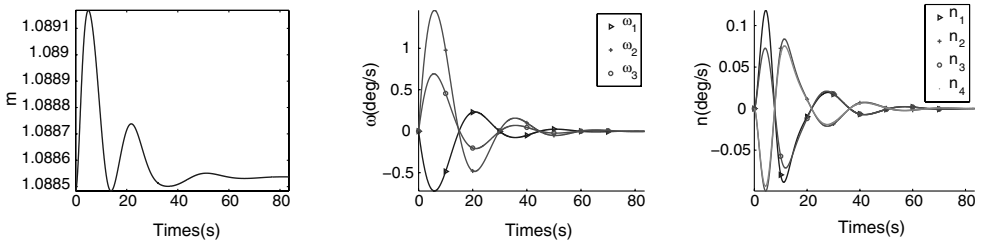

d) Singularity measure e) Angular velocity f) Null motion

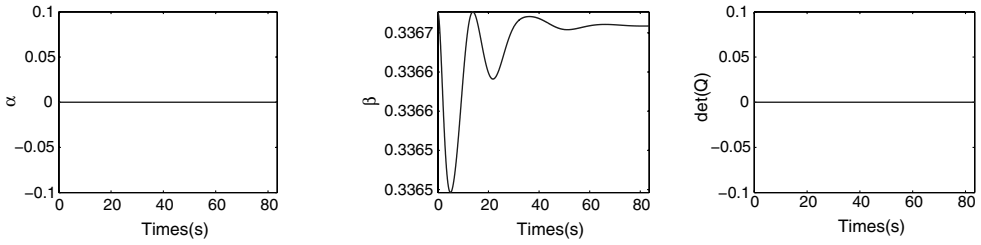

g) α h) β i) *det*(Q)

Fig. 4 Simulation results for LG, with $\alpha_0 = a = b = \mu_1 = 0$ and $\mu_2 = \beta_0 = 1$ at zero momentum.

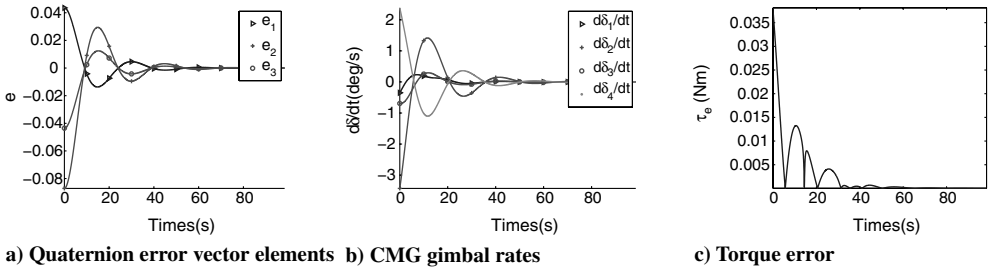

a) Quaternion error vector elements b) CMG gimbal rates c) Torque error

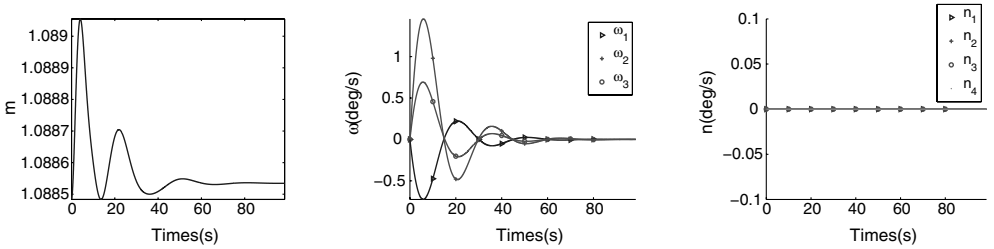

d) Singularity measure e) Angular velocity f) Null motion

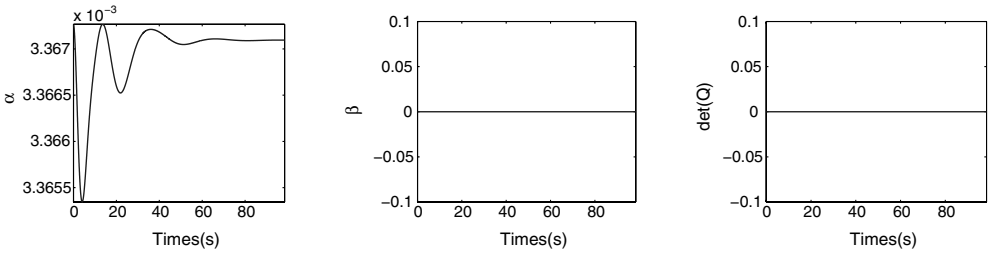

g) α h) β i) *det*(Q)

Fig. 5 Simulation results for SDA, with $\alpha_0 = 0.01$, $\beta_0 = a = b = \mu_2 = 0$, and $\mu_1 = 1$ at zero momentum.

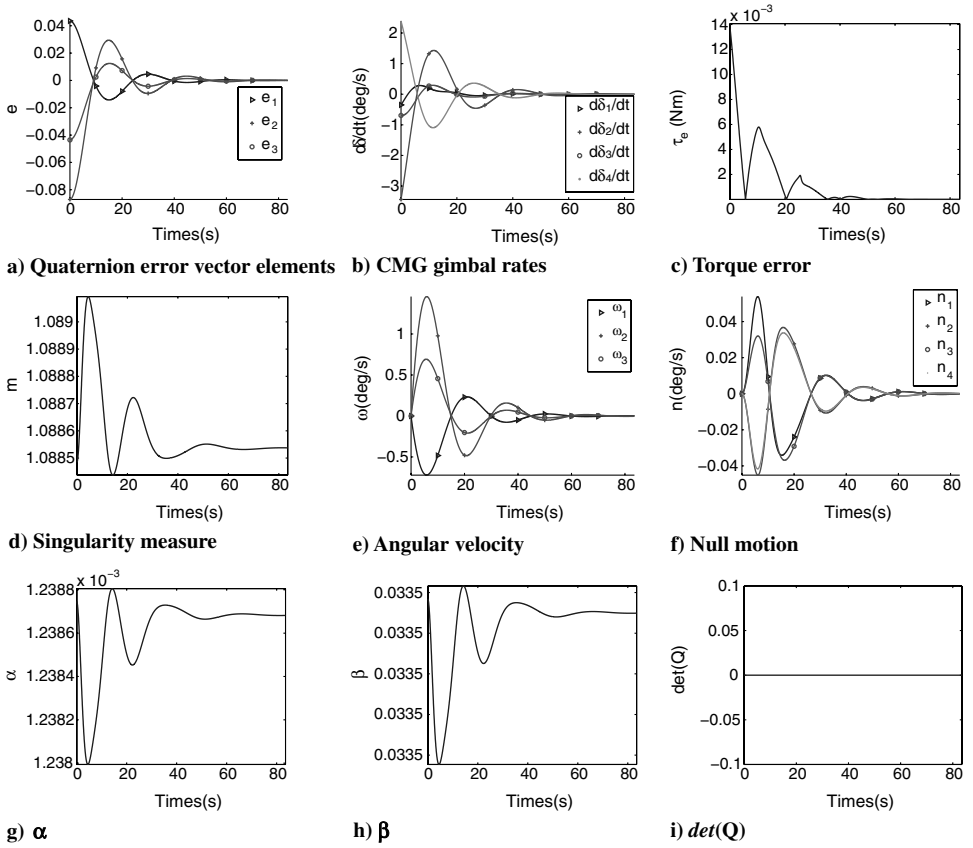

a) Quaternion error vector elements **b) CMG gimbal rates** **c) Torque error**

d) Singularity measure **e) Angular velocity** **f) Null motion**

g) α **h) β** **i) *det*(Q)**

Fig. 6 Simulation results for HSL, with $\alpha_0 = 0.01$, $\beta_0 = 2$, $a = 1$, $b = 3$, and $\mu_1 = \mu_2 = 1$ at zero momentum.

1. Local-Gradient Simulation Results

The parameters for this simulation are $\alpha_0 = a = b = \mu_1 = 0$ and $\mu_2 = \beta_0 = 1$. The plots in Fig. 7b show that the LG method unsuccessfully avoids this elliptic saturation singularity with the use of finite gimbal accelerations and implementable gimbal rates. Null motion in Fig. 7f is not the cause of these large gimbal rates and infinite accelerations. The reason that these gimbal rates are so large is completely due to the singularity in the Moore–Penrose inverse associated with the forced part of the gimbal solution. This is because the LG methods use only null motion for singularity avoidance, and there does not exist a null-motion solution to avoid elliptic singularities. Encounter of elliptic singularity is verified from the positive result shown in Fig. 7i.

2. Singular-Direction-Avoidance Simulation Results

The parameters for this simulation are $\alpha_0 = 0.01$, $\beta_0 = a = b = \mu_2 = 0$, and $\mu_1 = 1$. The SDA method escapes the elliptic saturation singularity, as shown in Fig. 8d, with torque error shown in Fig. 8c. This singularity is verified to be elliptic from the positive result shown in Fig. 8i.

3. Hybrid-Steering-Logic Simulation Results

The parameters for this simulation are $\alpha_0 = 0.01$, $\beta_0 = 2$, $a = 1$, $b = 3$, and $\mu_1 = \mu_2 = 1$. The HSL method has similar results to that of the SDA method but has a smaller amount of torque error, shown in Fig. 9c. Also, the parameters α and β in Figs. 9g and 9h show how torque error is added when at the elliptic saturation singularity with less null motion (i.e., less null motion, because the internal singularity is elliptic). This singularity is verified to be elliptic from the positive result shown in Fig. 9i.

D. Case 3: Near Hyberbolic Internal Singularities

The final set of simulations starts at initial gimbal angles $\delta = [15 \quad 105 \quad 195 \quad -75]^T$ deg near an hyperbolic internal singularity (i.e., a distance 15 deg from each CMG away from the internal singularity at $\delta = [0 \quad 90 \quad 180 \quad -90]^T$ deg).

1. Local-Gradient Simulation Results

The parameters for this simulation are $\alpha_0 = a = b = \mu_1 = 0$ and $\mu_2 = \beta_0 = 1$. The LG method, by itself here, is able to avoid the hyperbolic internal singularity without the use of torque error, as shown in Figs. 10c and 10d. This singularity is verified to be hyperbolic from the negative result shown in Fig. 10i.

2. Singular-Direction-Avoidance Simulation Results

The parameters for this simulation are $\beta_0 = a = b = \mu_2 = 0$, $\mu_1 = 1$, and $\alpha_0 = 0.01$. The gimbal rates for this method, shown in Fig. 11b, are 10 times smaller than that for the LG method. The SDA method escapes the hyperbolic internal singularity successfully, with torque error as shown in Figs. 11c and 11d. The added torque error for singularity escape versus null motion for singularity avoidance is the tradeoff between SDA and LG. This singularity is verified to be hyperbolic from the negative result shown in Fig. 11i.

3. Hybrid-Steering-Logic Simulation Results

The parameters for this simulation are $\alpha_0 = 0.01$, $\beta_0 = 2$, $a = 1$, $b = 3$, and $\mu_1 = \mu_2 = 1$. Precision with the threat of hyperbolic internal singularities is the real strength of this method. Here, the torque error added is almost an order of magnitude less than that of the SDA method, as shown in Fig. 12c. Hyperbolic internal singularity is not approached, as shown in Fig. 12d. Also, the null motion added in Fig. 12f is an order of magnitude less than that of the LG method. This shows that the HSL method commands smaller gimbal rates for singularity avoidance. Therefore, HSL relies on null motion for singularity avoidance rather than trying to pass through the hyperbolic internal singularities as SDA, singularity robust inverse (SR), and generalized SR do. This singularity is verified to be hyperbolic from the zero result shown in Fig. 12i.

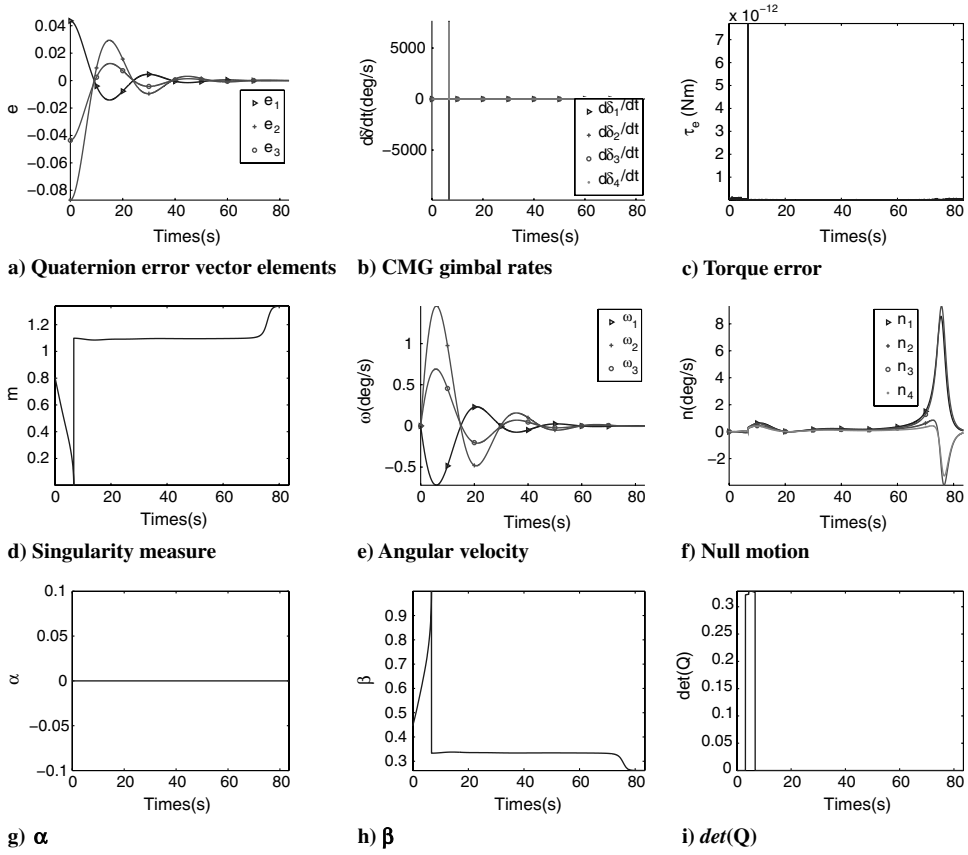

a) Quaternion error vector elements b) CMG gimbal rates c) Torque error

d) Singularity measure e) Angular velocity f) Null motion

g) α h) β i) *det*(Q)

Fig. 7 Simulation results for LG, with $\alpha_0 = a = b = \mu_1 = 0$ and $\mu_2 = \beta_0 = 1$ near internal elliptic singularities.

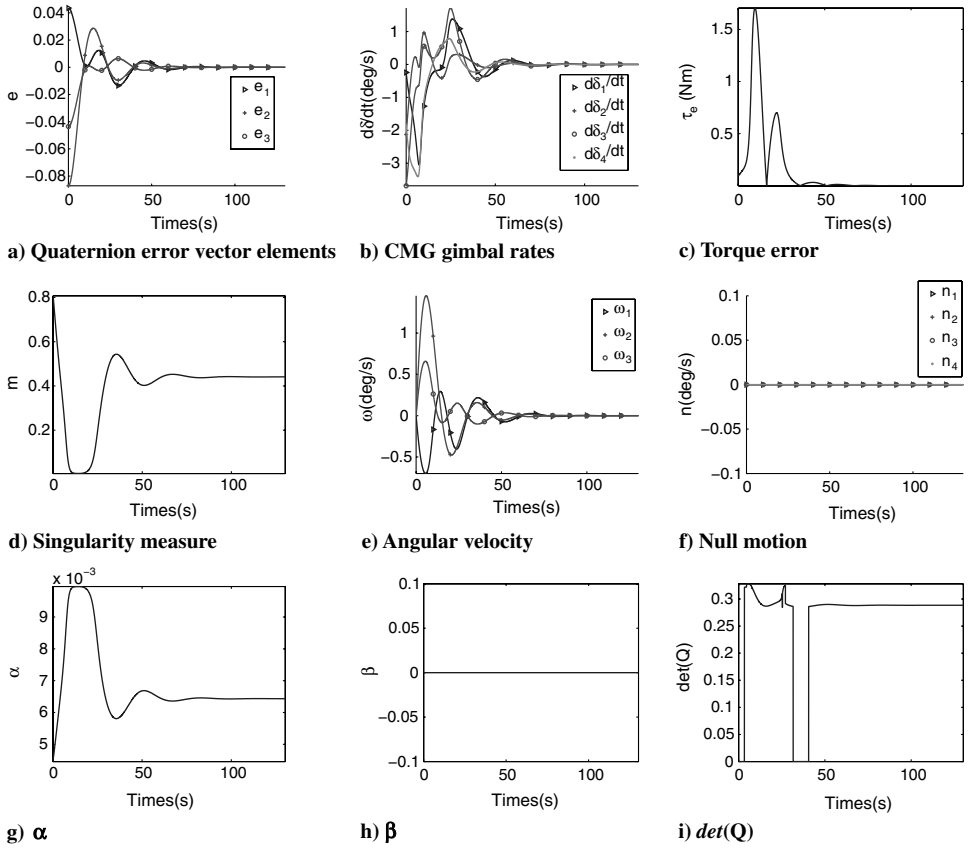

a) Quaternion error vector elements b) CMG gimbal rates c) Torque error

d) Singularity measure e) Angular velocity f) Null motion

g) α h) β i) *det*(Q)

Fig. 8 Simulation results for SDA, with $\alpha_0 = 0.01$, $\beta_0 = a = b = \mu_2 = 0$, and $\mu_1 = 1$ near internal elliptic singularities.

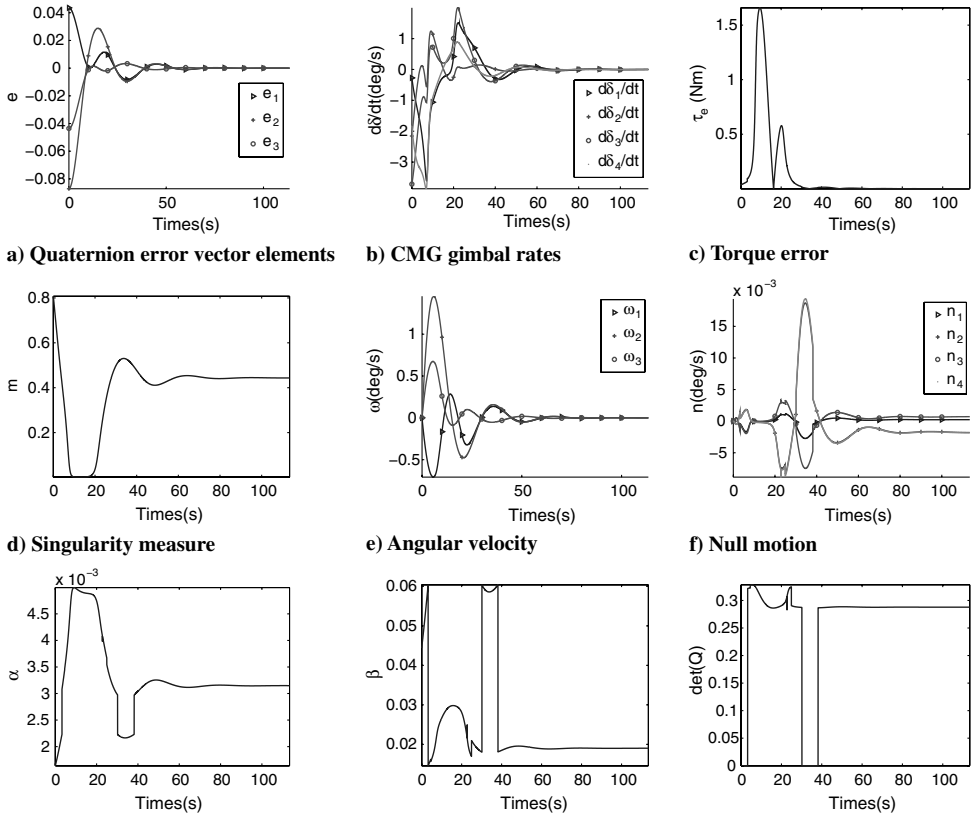

a) Quaternion error vector elements b) CMG gimbal rates c) Torque error

d) Singularity measure e) Angular velocity f) Null motion

g) α h) β i) *det*(Q)

Fig. 9 Simulation results for HSL, with $\alpha_0 = 0.01$, $\beta_0 = 2$, $a = 1$, $b = 3$, and $\mu_1 = \mu_2 = 1$ near internal elliptic singularities.

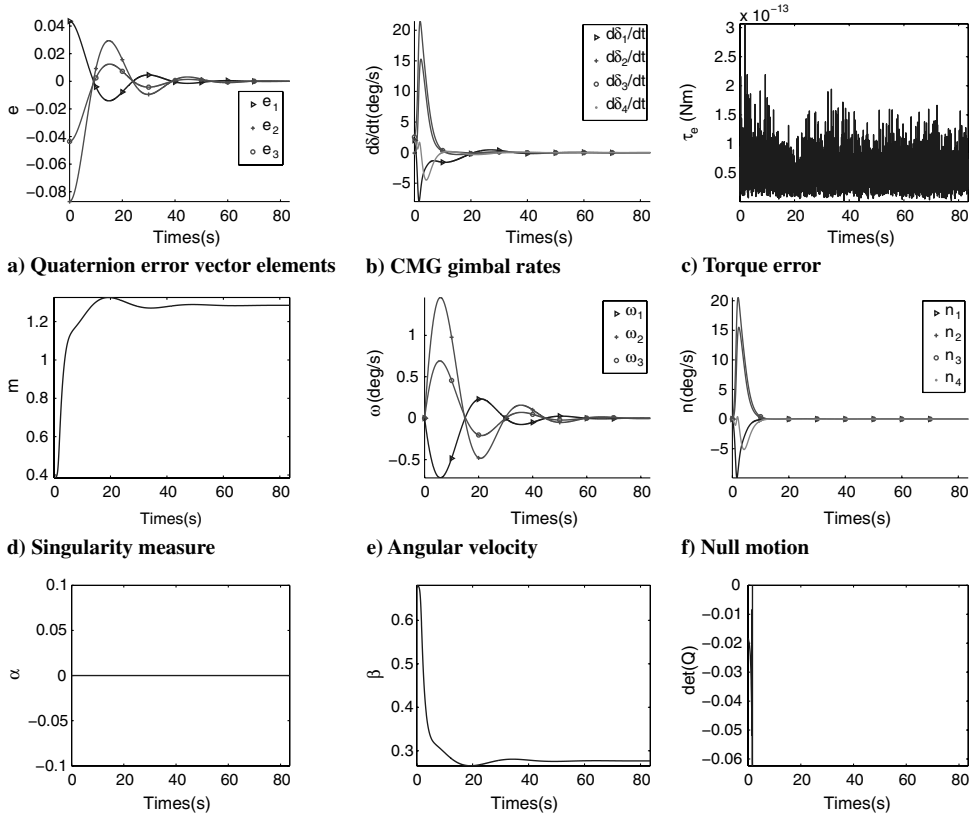

a) Quaternion error vector elements b) CMG gimbal rates c) Torque error

d) Singularity measure e) Angular velocity f) Null motion

g) α h) β i) *det*(Q)

Fig. 10 Simulation results for LG, with $\alpha_0 = a = b = \mu_1 = 0$ and $\mu_2 = \beta_0 = 1$ near internal hyperbolic singularities.

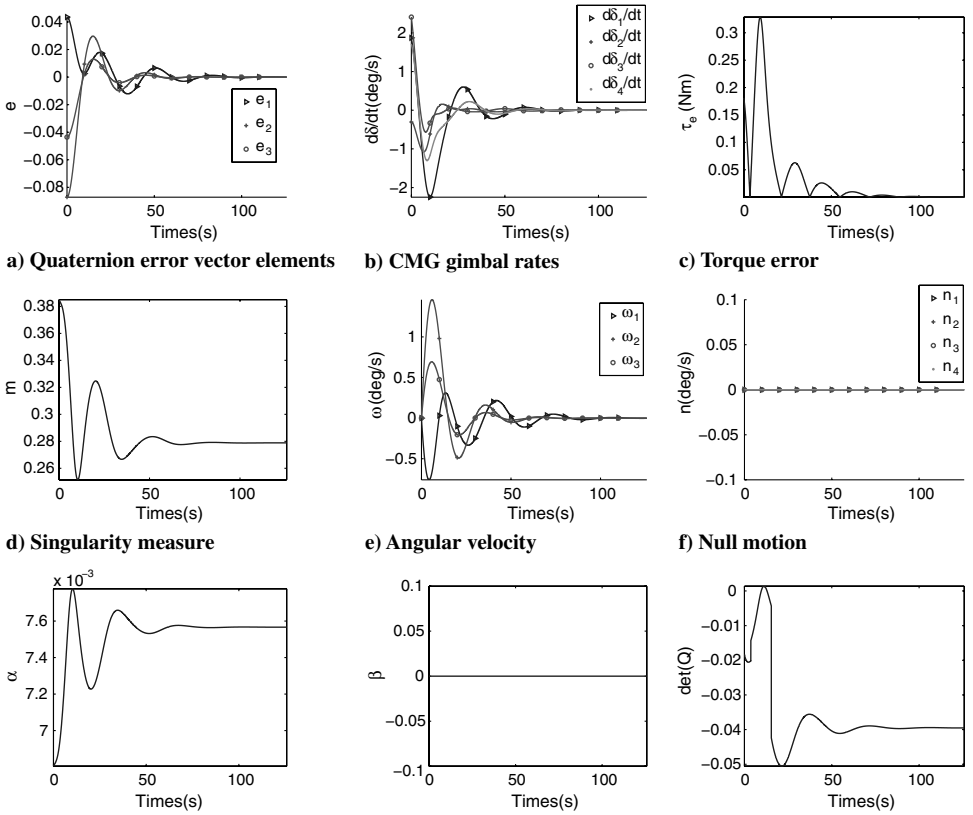

a) Quaternion error vector elements b) CMG gimbal rates c) Torque error

d) Singularity measure e) Angular velocity f) Null motion

g) α h) β i) *det*(Q)

Fig. 11 Simulation results for SDA, with $\alpha_0 = 0.01$, $\beta_0 = 0$, $a = 0$, $b = 0$, and $\mu = 1$ near internal hyperbolic singularities.

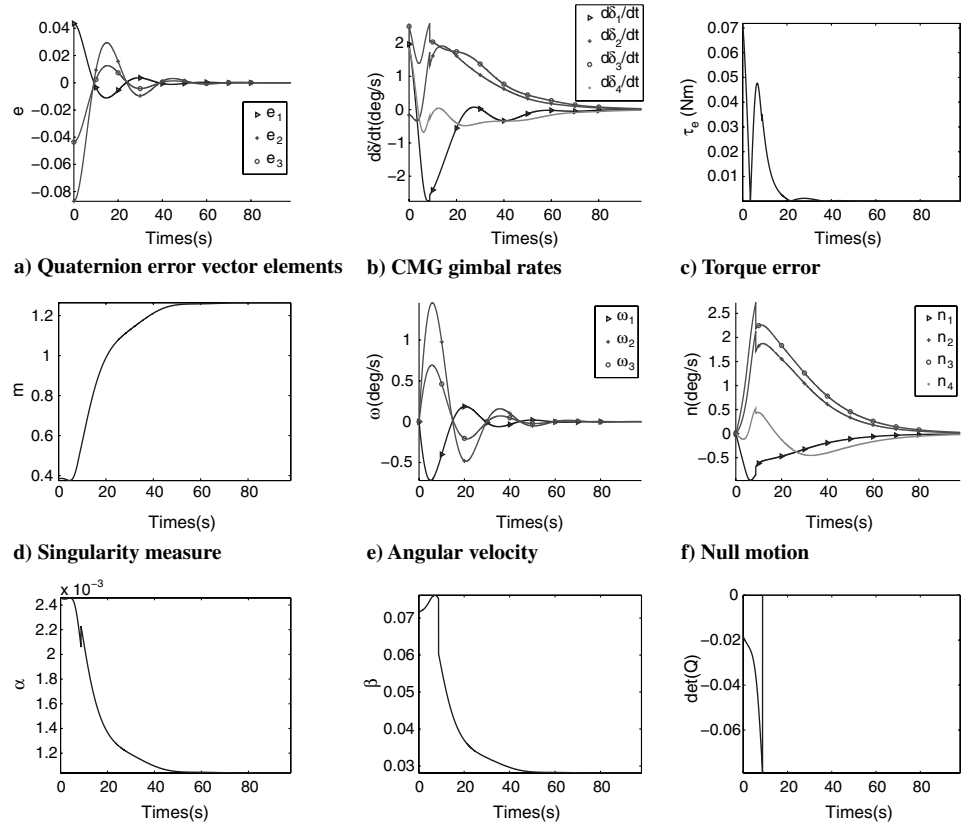

a) Quaternion error vector elements b) CMG gimbal rates c) Torque error

d) Singularity measure e) Angular velocity f) Null motion

g) α h) β i) *det*(Q)

Fig. 12 Simulation results for HSL, with $\alpha_0 = 0.01$, $\beta_0 = 2$, $a = 1$, $b = 3$, and $\mu_1 = \mu_2 = 1$ near internal hyperbolic singularities.

VI. Conclusions

The development of a novel HSL that increases attitude tracking performance of SGCMGs is discussed and exploits the use of LG and pseudoinverse methods, specifically SDA. The novelty of the approach is attributed to the definitions of new internal singularity metrics that allow continuous transition between singularity avoidance and singularity escape methods, depending on the type of singularity encountered. For hyperbolic internal singularities, a singularity avoidance strategy using LG methods is used, whereas for elliptic singularities (both external and internal), a pseudoinverse strategy using SDA is used.

Through analysis and simulation, it is shown that HSL performs better than SDA at hyperbolic singularity, as good as SDA at elliptic singularities, and is able to handle both hyperbolic and elliptic singularities, unlike LG. In addition, the HSL at hyperbolic internal singularities with a small amount of torque error requires gimbal rates an order of magnitude less than LG (i.e., less null motion with some torque) while still avoiding the hyperbolic internal singularity. Finally, HSL is successful in avoiding hyperbolic internal and elliptic internal and external singularities while reducing the amount of torque error at hyperbolic singularities when compared with legacy singularity escape methods. Furthermore, through simulations, it is shown that HSL with small additions of torque error requires gimbal rates an order of magnitude smaller than that required for the pure LG method (i.e., less null motion at the expense of some torque error).

References

[1] Hall, C., "Integrated Spacecraft Power and Attitude Control Systems Using Flywheels," U.S. Air Force Institute of Technology TR 000, 1997.

[2] Kennel, H., "A Control Law for Double-Gimballed Control Moment Gyros Used for Space Vehicle Attitude Control," NASA TM 64536, 1970.

[3] Zhou, J., and Zhou, D., "Spacecraft Attitude Control with Double-Gimbaled Control Moment Gyroscopes," *2007 IEEE International Conference on Robotics and Biomimetics (ROBIO 2007)*, IEEE Publ., Piscataway, NJ, 2007, pp. 1557–1562.

[4] Powell, B., Lang, G., Lieberman, S., and Rybak, S., "Synthesis of Double Gimbal Control Moment Gyro Systems for Spacecraft Attitude Control," *AIAA Guidance, Control, and Flight Mechanics Conference*, AIAA Paper 1971-937, 1971.

[5] Jansen, R., "Single Axis Flywheel IPACS @1300 W, 0.8 Nm," *NASA Space Power Workshop*, NASA, April 2005.

[6] Notti, J., Cormack, A., and Klein, W., "Integrated Power/Attitude Control System (IPACS)," *Journal of Spacecraft and Rockets*, Vol. 12, No. 8, 1975, pp. 485–491. doi:10.2514/3.57006

[7] DeVon, D., Fuentes, R., and Fausz, J., "Closed-Loop Power Tracking for an Integrated Power and Attitude Control System Using Variable-Speed Control Moment Gyroscopes," AIAA Guidance, Navigation, and Control Conference and Exhibit, AIAA, Paper 2004-5130, Aug. 2004.

[8] Fausz, J., and Richie, D., "Flywheel Simultaneous Attitude Control and Energy Storage Using a VSCMG Configuration," *Proceedings of the 2000 IEEE International Conference on Control Applications, 2000*, IEEE Publ., Piscataway, NJ 2000, pp. 991–995.

[9] Babuska, V., Beatty, S., deBlonk, B., and Fausz, J., "A Review of Technology Developments in Flywheel Attitude Control and Energy Transmission Systems," *Proceedings of the IEEE Aerospace Conference*, Vol. 4, IEEE Publ., Piscataway, NJ, 2004, pp. 2784–2800.

[10] Margulies, G., and Aubrun, J., "Geometric Theory of Single-Gimbal Control Moment Gyro Systems," *Journal of the Astronautical Sciences*, Vol. 26, No. 2, 1978, pp. 159–191.

[11] Schaub, H., Vadali, S., and Junkins, J., "Feedback Control Law for Variable Speed Control Moment Gyros," *Journal of the Astronautical Sciences*, Vol. 46, No. 3, 1998, pp. 307–328.

[12] Schaub, H., and Junkins, J., "Singularity Avoidance Using Null Motion and Variable-Speed Control Moment Gyros," *Journal of Guidance, Control, and Dynamics*, Vol. 23, No. 1, 2000, pp. 11–16. doi:10.2514/2.4514

[13] Schaub, H., and Junkins, J., "CMG Singularity Avoidance Using VSCMG Null Motion," AIAA/AAS Astrodynamics Specialist Conference and Exhibit, Boston, MA, AIAA Paper 1998-4388, 1998.

[14] Yoon, H., and Tsiotras, P., "Singularity Analysis and Avoidance of Variable-Speed Control Moment Gyros-Part 2: Power Constraint Case," AIAA Guidance, Navigation, and Control Conference, Providence, RI, AIAA Paper 2004-5208, 2004.

[15] Yoon, H., and Tsiotras, P., "Singularity Analysis of Variable-Speed Control Moment Gyros," *Journal of Guidance, Control, and Dynamics*, Vol. 27, No. 3, 2004, pp. 374–386. doi:10.2514/1.2946

[16] Kurokawa, H., "A Geometric Study of Single Gimbal Control Moment Gyros," Ph.D. Thesis, Univ. of Tokyo, 1998.

[17] Wie, B., "," U.S. Patent Application for "Singularity Escape/Avoidance Steering Logic for Control Moment Gyro Systems," Docket No. 10-652,219, 28 Aug. 2003.

[18] Bedrossian, N., Paradiso, J., Bergmann, E., and Rowell, D., "Steering Law Design for Redundant Single-Gimbal Control Moment Gyroscopes," *Journal of Guidance, Control, and Dynamics*, Vol. 13, No. 6, 1990, pp. 1083–1089. doi:10.2514/3.20582

[19] Cornick, D. E., "Singularity Avoidance Control Laws for Single Gimbal Control Moment Gyros," AIAA Paper 1979-1698, 1979.

[20] Hefner, R. D., and McKenzie, C. H., "A Technique for Maximizing the Torque Capability of Control Moment Gyro Systems," *Astrodynamics*, Vol. 54, No. 83-387, 1983, pp. 905–920.

[21] Kuhns, M., and Rodriguez, A., "A Preferred Trajectory Tracking Steering Law for Spacecraft with Redundant CMGs," *Proceedings of the American Control Conference*, Vol. 5, No. , June 1995, pp. 3111–3115.

[22] Wie, B., *Space Vehicle Dynamics and Control* 2nd ed., AIAA, Reston, VA, 2008, pp. 463–469.

[23] Paradiso, J., "Global Steering of Single Gimballed Control Moment Gyroscopes Using a Directed Search," *Journal of Guidance, Control, and Dynamics*, Vol. 15, No. 5, 1992, pp. 1236–1244. doi:10.2514/3.20974

[24] Paradiso, J., "A Search-Based Approach to Steering Single Gimballed CMGs," NASA TR CSDL-R-2261, 1991.

[25] Peck, M., Hamilton, B., and Underhill, B., U.S. Patent Application for "Method and System for Optimizing Torque in a CMG Array," Docket No. 10-903,774, 30 July 2004.

[26] Bailey, D., Heiberg, C., and Wie, B., U.S. Patent 6,131,056 for "Continuous Attitude Control that Avoids CMG Array Singularities," 10 Oct. 2000.

[27] Elgersma, M., Johnson, D., Peck, M., Underhill, B., Stein, G., Morton, B., and Hamilton, B., "Method and System for Controlling Sets of Collinear Control Moment Gyroscopes," US Patent App. 11-291,706, 10 Oct. 2000.

[28] Jones, L., and Peck, M., "A Generalized Framework for Linearly-Constrained Singularity-Free Control Moment Gyro Steering Laws," AIAA Guidance, Navigation and Control Conference, AIAA Paper 2009-5903, 2009.

[29] Kurokawa, H., "Constrained Steering Law of Pyramid-Type Control Moment Gyros and Ground Tests," *Journal of Guidance, Control, and Dynamics*, Vol. 20, No. 3, 1997, pp. 445–449. doi:10.2514/2.4095

[30] Nakamura, Y., and Hanafusa, H., "Inverse Kinematic Solutions with Singularity Robustness for Robot Manipulator Control," *Journal of Dynamic Systems, Measurement and Control*, Vol. 108, No. 3, 1986, pp. 163–171. doi:10.1115/1.3143764

[31] Wie, B., Bailey, D., and Heiberg, C., "Singularity Robust Steering Logic for Redundant Single-Gimbal Control Moment Gyros," *Journal of Guidance, Control, and Dynamics*, Vol. 24, No. 5, 2001, pp. 865–872. doi:10.2514/2.4799

[32] Wie, B., Bailey, D., and Heiberg, C., "Rapid Multitarget Acquisition and Pointing Control of Agile Spacecraft," *Journal of Guidance, Control, and Dynamics*, Vol. 25, No. 1, 2002, pp. 96–104. doi:10.2514/2.4854

[33] Ford, K., and Hall, C., "Singular Direction Avoidance Steering for Control-Moment Gyros," *Journal of Guidance, Control, and Dynamics*, Vol. 23, No. 4, 2000, pp. 648–656. doi:10.2514/2.4610

[34] Vadali, S., Oh, H., and Walker, S., "Preferred Gimbal Angles for Single Gimbal Control Moment Gyros," AIAA Guidance, Navigation and Control Conference, Boston, MA, AIAA Paper 1989-3477, 1989.

[35] Leve, F., "Development of the Spacecraft Orientation Buoyancy Experimental Kiosk," M.S. Thesis, Univ. of Florida, 2008.

[36] Larson, W., and Wertz, J., *Space Mission Analysis and Design*, 3rd ed., Microcrosm, Bloomington, IN, 1999, p. 359.